Science Bulletin 65 (2020) 477–485

Contents lists available at ScienceDirect

Science Bulletin

journal homepage: www.elsevier.com/locate/scib

Science Bulletin
www.scibull.com

Article

# Lateral bipolar photoresistance effect in the CIGS heterojunction and its application in position sensitive detector and memory device

Jihong Liu [a,1], Zicai Zhang [a,1], Shuang Qiao [a,b,*], Guangsheng Fu [a], Shufang Wang [a,*], Caofeng Pan [b,c,*]

[a] Hebei Key Laboratory of Optic-Electronic Information and Materials, College of Physics Science and Technology, Hebei University, Baoding 071002, China
[b] Beijing Key Laboratory of Micro-nano Energy and Sensor, Beijing Institute of Nanoenergy and Nanosystems, Chinese Academy of Sciences, Beijing 100083, China
[c] College of Physics and Optoelectronic Engineering, Shenzhen University, Shenzhen 518060, China

ARTICLE INFO

*Article history:*
Received 7 September 2019
Received in revised form 23 October 2019
Accepted 8 November 2019
Available online 18 November 2019

*Keywords:*
CIGS heterostructure
Lateral photoresistance
Photoresponse
Position sensitive detector

ABSTRACT

$Cu(In,Ga)Se_2$ (CIGS) based multilayer heterojunction, as one of the best high efficiency thin film solar cells, has attracted great interest due to its outstanding features. However, the present studies are primarily focused on the structure optimization and modulation in order to enhance the photoelectric conversion efficiency. Here, we exploit another application of this multilayer heterostructure in photoresistance-modulated position sensitive detector by introducing lateral photoresistance effect. The lateral photoresistance measurements show that this multilayer heterojunction exhibits a wide spectral response (~330 to ~1150 nm) and excellent bipolar photoresistance performances (position sensitivity of ~63.26 Ω/mm and nonlinearity <4.5%), and a fast response speed (rise and fall time of ~14.46 and ~14.42 ms, respectively). More importantly, based on the lateral photoresistance effect, the CIGS heterostructure may also be developed as a position-dependent resistance memory device, which can be modulated by changing laser intensity, wavelength, and bias voltage with excellent stability and repeatability, and the position resolution reaches up to 1 μm. These results can be well explained by considering the diffusion and the drift model of carriers in the CIGS multilayer heterojunction. This work provides a new approach of achieving novel photoelectric sensors and memory devices based on the traditional photovoltaic heterostructures.



## 1. Introduction

With the development of photoelectric technology, thermal or pressure imaging, energy storage and environmental monitoring, high sensitive, fast speed and broadband photoelectric sensors are increasingly needed and have attracted great attention in the world [1–8]. From the previous results, most of devices work in the photovoltaic principle, thus some of photovoltaic materials have been exploited into high performance photodetectors [9–12]. Recently, $Cu(In,Ga)Se_2$ (CIGS), as a polycrystalline chalcopyrite, has been observed to be one of the best photoelectric materials due to its numerous exciting properties [13–15]. And the CIGS multilayer heterojunction has achieved great attention as one of the mature film solar cells considering its high photovoltaic efficiency and low-cost in manufacture [16,17]. However, the previous researches have been mainly focused on the structure optimization and modulation as solar cells in order to enhance the efficiency. Even though some of photovoltaic structures have been successfully developed as photoelectric devices, they operate on either voltage or current responses [7,12,18], while the photo-induced resistance sensors were still seldomly reported. More importantly, resistance reflects an inherent characteristic of a given material, thus the devices worked by modulating the resistances have attracted great interest and been thought to show significant applications.

Since the lateral photovoltaic effect (LPE) had been discovered in 1930 [19], it has aroused much attention and been studied in many structures duo to its promising prospect in position sensitive detectors (PSD) [20–26]. Considering the carrier gradient and diffusion in the LPE, this effect may also be utilized to tune the resistance of the device by changing the transportation or intrinsic scattering of the drift carriers [27,28], thus to exploit photoresistance-induced PSDs as similar as the LPE [29–31], calling as lateral photoresistance effect (LPRE). More importantly, based on the LPRE, the heterojunction may also be developed as position-dependent memory devices of the resistance.

Here, the Mo/CIGS/CdS/ZnO/ITO multilayer heterojunction was prepared on the glass substrate. Based on LPRE, we exploit it as a

* Corresponding authors.
*E-mail addresses:* sqiao@hbu.edu.cn (S. Qiao), sfwang@hbu.edu.cn (S. Wang), cfpan@binn.cas.cn (C. Pan).
[1] These authors contributed equally to this work.

https://doi.org/10.1016/j.scib.2019.11.016
2095-9273/

sensitive, fast response and broadband photoresistance-modulated PSD. It is found that the surface resistance of this multilayer heterostructure, which is linearly related to the laser position, exhibits a bipolar behavior and the resistance sensitivity improves gradually with increasing illumination power under a constant bias. Besides, the heterojunction can also be developed as a position-dependent resistance memory device by controlling the laser intensity, wavelength and bias voltage with position resolution up to 1 μm. Scattering modulation of the ITO layer resistance by the photo-generated carriers in the CIGS multilayer heterojunction was proposed to successfully explain these results. Our work puts forward an insight for constructing innovative photoelectric detectors according to the photo-induced resistance effect.

## 2. Experimental

### 2.1. CIGS heterojunction preparation

A 3.2 mm-thick soda-lime glass was used as the substrate. The Mo, CIGS, CdS, ZnO, and ITO layers were deposited on the substrate layer by layer, respectively, and the preparation details can be obtained in Refs. [26,32]. Finally, two Ag point electrodes (diameter of ~0.5 mm), which are defined as electrode A and electrode B, were evaporated on the ITO layer with a 1.3 mm-distance controlling by a mask.

### 2.2. Electrical and optical properties

The current-voltage (*I-V*) characteristics were measured by a SourceMeter (Keithley 2400) or a home-made system with a voltage source (SR560), a current source (SR570) and a 671 nm-laser. External quantum efficiency (EQE) was evaluated by a QTest station (CROWNTECH, 500AD) equipped with a 150 W Xenon lamp, an integrating sphere and a SR830 lock-in amplifier.

### 2.3. LPRE and response speed measurements

The LPRE was identified by a home-made system equipped with a SourceMeter (Keithley 2400), a motorized linear stage (minimum step length of 1 μm), and several lasers with wavelengths of 405, 532, 671, 808, and 980 nm, respectively. The time-response of the CIGS multilayer heterojunction was identified by a current and voltage source (SR570 and SR560), and an optical chopper.

## 3. Results and discussion

The *I-V* curve of the CIGS multilayer heterojunction between the top A electrode and back Mo layer, which exhibits a clear rectification characteristic, is presented in Fig. 1a, indicating the well p-n behavior of the heterojunction. Fig. 1b gives the transverse *I-V* result between the A and B electrodes. The linear relationship demonstrates that the Ag electrodes come into being the Ohmic contacts with the ITO layer. Moreover, the resistance (*R*) of the ITO layer keeps at ~108.2 Ω nearly without depending on the bias. The photoresponses of the CIGS multilayer heterojunction suggest that the photocurrent increases quickly with illumination powers within our measurement range even to ~30 mW of a 671 nm-laser, as shown in Fig. 1c. Fig. 1d gives the EQE result, which shows the broadband response range of the device from ~330 to ~1150 nm.

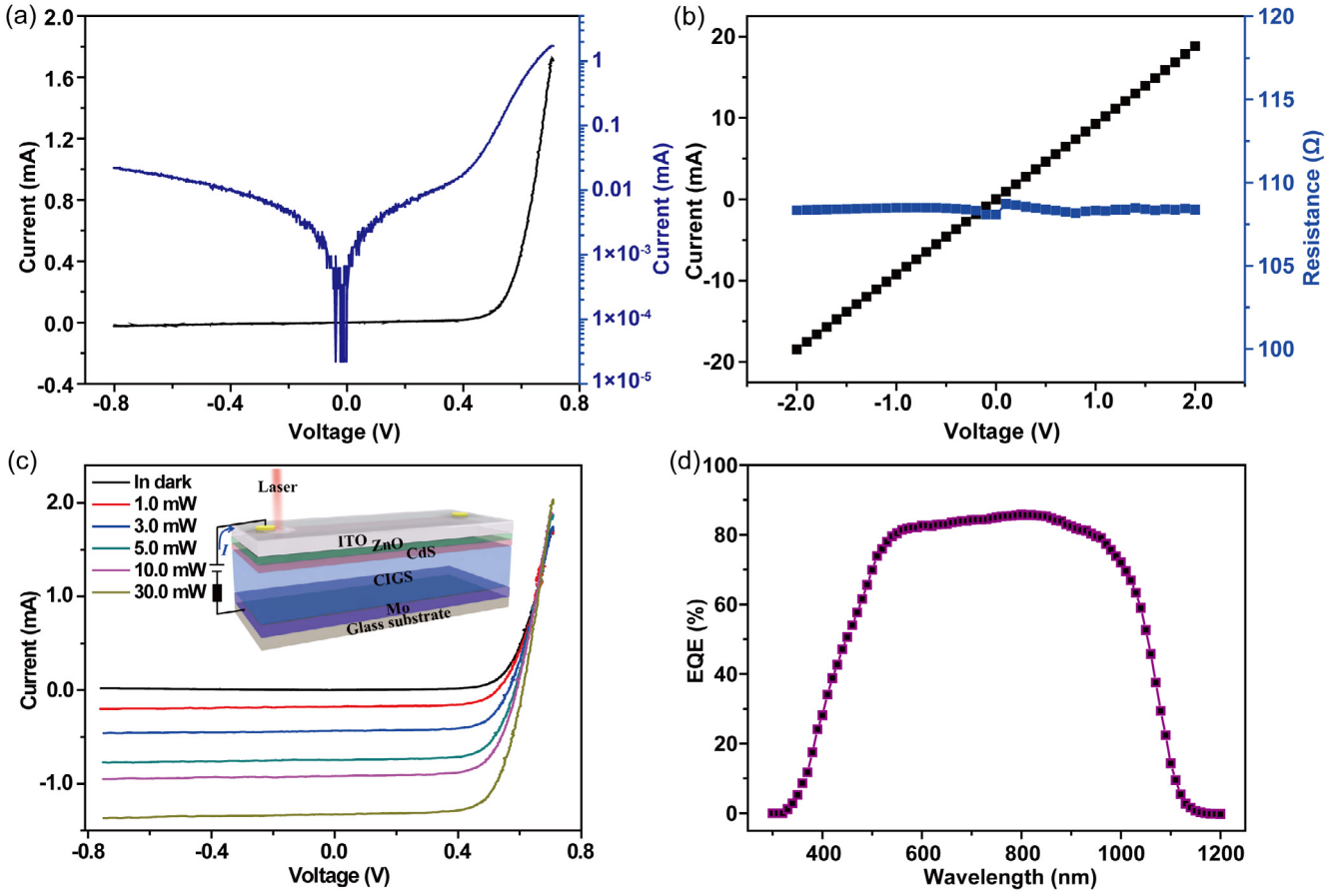


**Fig. 1.** (Color online) The longitudinal *I-V* result (a) and the transverse *I-V* and *R-V* results (b) of the CIGS multilayer heterojunction. (c) Photoresponse results of the heterojunction measured under illumination of a 671 nm-laser with 1, 3, 5, 10, 30 mW, respectively. (d) EQE spectra of the CIGS multilayer heterojunction.

The LPRE schematic diagram of the CIGS multilayer heterojunction is presented in Fig. 2a and b. Under illumination of a suitable laser beam, electron-hole pairs would be generated in the CIGS layer and separated and swept to the top and bottom layers by the interface field, respectively, resulting in lots of carriers gathering at the illumination position. Then, these carriers diffuse to right and left sides immediately, and the original movement of the drift carriers from B(/A) side to A(/B) side under external bias would be accelerated or decelerated due to the enhanced or weakened scattering effect, respectively [29–31]. When the laser beam moves gradually from A side to B side, the lengths of the accelerated and decelerated regions would be regularly tuned, thus a photoresistance curve as a function of the position of the laser beam is gotten. To well clarify the bias polarity effect, the external bias is divided into positive and negative biases based on the connection modes of $A^+$ ($B^-$) and $A^-$ ($B^+$), respectively. Fig. 2c gives the laser position-dependent photoresistance curves under 10 mW illumination of a 671 nm-laser with applying ±0.5 V biases. It is obtained that the photoresistance shows a clear linear dependence on the laser position between A and B region, with reversed and symmetrical changing tendency, meaning that the photoresistance decreases from a maximum ($R_{max}$) to a minimum ($R_{min}$) with laser beam moving from A to B under positive bias, but increases from the $R_{min}$ to the $R_{max}$ under negative bias. Considering the linear dependence of the photoresistance on the position of the laser beam, it is suggested that the LPRE can also be utilized to exploit resistance-modulated PSD devices as similar as the LPE [29–31].

Firstly, we evaluated the laser position-dependent resistance curves with biases of ±0.5 V and a 671 nm-laser illumination (with power changing from 1 to 30 mW), as presented in Fig. 3a and b, respectively. The $R_{max}$ increases and the $R_{min}$ decreases clearly with increasing laser powers (that is the photoresistance change improves), and the photoresistance depends linearly on the laser position in low powers (less than ~15 mW). However, the lateral photoresistance curves start to deviate from the linear behavior with increasing illumination power again and this phenomenon gets worse for larger powers. To judge the performance of this CIGS mutilayer heterojunction as a LPRE-based PSD, two key parameters referring to the LPE were proposed as position sensitivity and nonlinearity. The position sensitivity of the photoresistance can be extracted through the linear fitting, while the nonlinearity, which shows the deviation degree of the measured data from the normal linear results, can be deduced by the following equation [29,31]:

$$\text{Nonlinearity}\ (\%) = \frac{2 \times \sqrt{\frac{\left[\sum_{i=1}^{N}\left(R_i - R_i^L\right)^2\right]}{N}}}{|AB|} \times 100\%, \quad (1)$$

where |AB| is the distance between A and B, $N$ represents the total number of the measured points, $R_i$ and $R_i^L$ are the measured photoresistance and linear fitted resistance of the $i$ point, respectively.

Fig. 3c gives the extracted power-dependent sensitivities and nonlinearities. The sensitivity improves slowly at first from 6.71 to 63.07 Ω/mm with illumination power changing from 1 to 15 mW, then rises quickly from 96.17 to 171.28 Ω/mm with power changing from 20 to 30 mW again. The slowly enhancement of sensitivity in low laser power range can be attributed to the increment of the photoexcited carriers, as shown in Fig. 1c. While the dramatic enhancement in high power range is mainly due to the nonlinearly increased $R_{max}$, which can be clearly seen from the nonlinearities, as it keeps at around 2% under lower power illuminations (less than ~15 mW), and then gets more and more worse (from 4.5% to 15.1%) with increasing illumination power again. Notably, the high sensitivities under illumination of large powers cannot represent the best performances of the device as it is at the expense of linearity (meaning that the high sensitivity is resulted from the large nonlinearity). Overall consideration, we think that the maximal sensitivity of this CIGS multilayer heterostructure for a high performance PSD should be 63.07 Ω/mm at 15 mW due to its good nonlinearity of 4.5%, and this power can be defined as the turning point of linear to nonlinear behavior.

Then, the relative response of the LPRE to different lasers has been studied. The lateral photoresistance results with a 0.5 V bias and a 5 mW illumination are shown in Fig. 3d. It is obvious that the

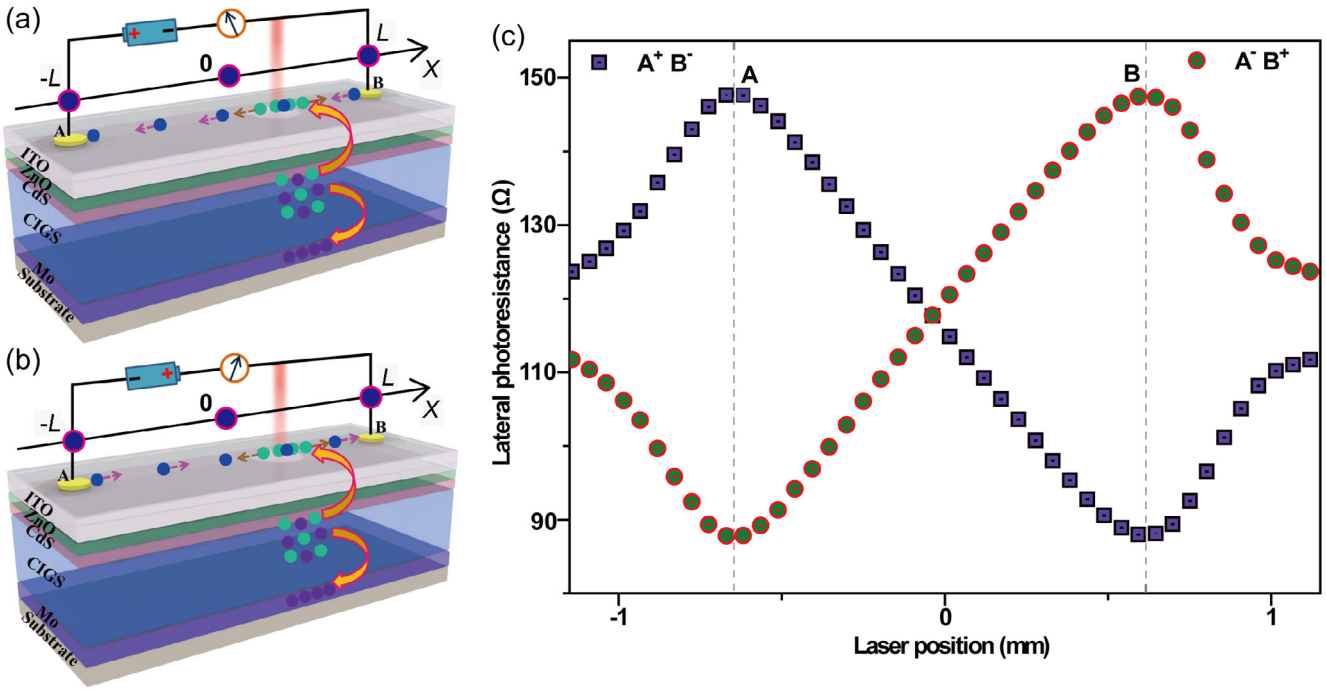


**Fig. 2.** (Color online) LPRE measurement diagram of the CIGS multilayer heterostructure under applying a positive bias (a) and a negative bias (b). (c) Typical laser position-dependent lateral photoresistance curves under illumination of a 671 nm-laser with 10 mW and applying biases of ±0.5 V.

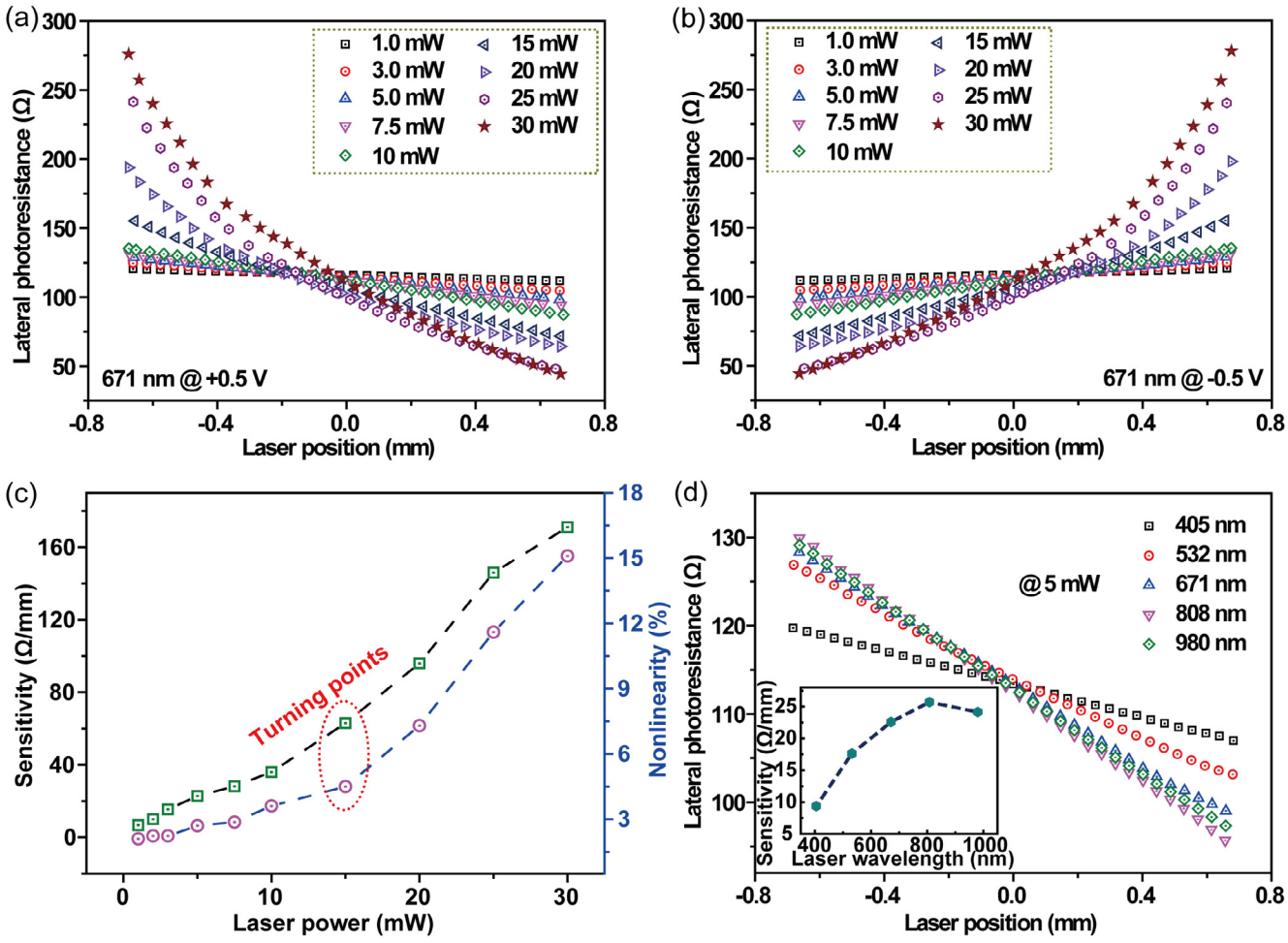


**Fig. 3.** (Color online) Laser position-dependent lateral photoresistance curves under illumination of a 671 nm-laser with different laser powers and applying bias of +0.5 V (a) and −0.5 V (b). (c) Extracted sensitivities and nonlinearities as a function of laser powers. (d) Laser position-dependent lateral photoresistance curves under illumination of different lasers with 5 mW, inset is the wavelength-dependent sensitivities.

lateral photoresistances are all linearly dependent on the position of the laser beam for all wavelengths, and the deduced sensitivity, which improves gradually with wavelength changing from 405 to 808 nm, and then decreases at 980 nm (inset of Fig. 3d), exhibits a strong wavelength dependence as similar as that of the EQE result, indicating the promising application of the CIGS multilayer heterojunction in the LPRE-modulated broadband PSD devices. Moreover, we also well studied the power-dependent LPRE under illumination of other lasers, and the lateral photoresistance curves at ±0.5 V are presented in Figs. S1 and S2 (online), respectively. Similar as that of the 671 nm-laser, the lateral photoresistance still shows a linear relationship with the position of the laser beam, and the response improves gradually with increasing laser power, and then the nonlinear behavior starts to appear when the illumination power adds to a certain value. However, the power turning point of the linear-to-nonlinear behavior is different for different lasers. To well illustrate this phenomenon, the sensitivities and the nonlinearities are also deduced, as shown in Fig. S3 (online). Generally, the sensitivity increases slowly when the nonlinearity is less than ~3%. However, when the nonlinearity exceeds 3%, the position sensitivity starts to get rapidly enhanced, suggesting the largely improved position sensitivity is indeed mainly attributed to the gradually deteriorated linearity. The turning points of the linear-to-nonlinear behavior (position sensitivity and nonlinearity) are circled in Fig. S3 (online). One can observe that the turning power decreases from ~50 to ~10 mW with wavelength increasing from 405 to 808 nm, and then rises to ~15 mW at 980 nm. Interestingly, although the turning power is different for different lasers, the corresponding sensitivities are all around 60 Ω/mm, implying that the linear-to-nonlinear behavior happens only when the number of the separated carriers gets a critical value for a constant bias (and the different turning points demonstrate the different photoexcited and separated efficiency of these wavelengths, which is consistent with the EQE result).

Then, to well understand the nonlinear behavior, the LPRE was then identified with adding different positive biases ranging from 0.15 to 10 V. Fig. S4a (online) shows the lateral photoresistance curves measured under 10 mW illumination of a typical 671 nm-laser. The lateral photoresistance curves are all nonlinear when the bias is lower than ~0.4 V (with position sensitivity of 63.26 Ω/mm at 0.4 V), and the nonlinearity increases drastically with decreasing external bias, as shown in Fig. S4b (online). This is similar to that of increasing powers as decreasing the number of drift electrons under low biases to some extent is equal to improving the number of diffusion electrons under large power illuminations, further confirming the crucial scattering effect of the diffusion carriers on the drift carriers. However, the lateral photoresistance starts to decrease linearly from a maximum to a minimum with laser beam moving from A side to B side when the bias is larger than ~0.4 V, but the lateral photoresistance response (/photoresistance sensitivity) decreases with increasing biases (Fig. S4b online). In particular, when the bias is larger than

~5 V, there seems no photoresistance change with changing the position of the laser beam (that is the resistance keeps nearly the same value as that without illumination) [33]. The lateral photoresistance curves were also measured under applying the corresponding negative biases and the deduced sensitivities and nonlinearities were gotten in Fig. S4c (online). The lateral photoresistance curves, as well as the sensitivities and nonlinearities, are symmetric to the zero point with that of the positive biases, indicating the intrinsic bipolar LPRE characteristic of this multilayer heterojunction. Moreover, the LPRE may also be developed in other photovoltaic structures, such as dye-sensitized solar cell or trandiitional Si/Ge solar cells [34,35].

Considering the laser position-dependent resistance effect, we think that this CIGS heterojunction may also be exploited as a laser-modulated resistance memory device. Fig. 4a gives a transient lateral photoresistance curve under a typical 5 mW illumination. The lateral photoresistance response stays constant for at least 24 cycles in the 48 s, suggesting the remarkable stability and repeatability of the device. With changing laser powers, the lateral photoresistance response decreases or increases correspondingly but still keeps very good stability, as shown in Fig. 4b. More importantly, it is indicated that this heterojunction can be used as a laser power-based resistance memory device. And there is no restriction of the nonlinearity (the dependence of the lateral photoresistance on the laser position) as the memory is based on the amplitude changing of the resistance, which is quite different from the PSD. Besides, the lateral photoresistance behaves clearly different responses for biases of ±0.5 V, especially for larger laser powers. In order to evaluate the bias effect, the transient lateral photoresistance curve is also measured with bias increasing from 0.15 to 10 V (Fig. 4c). The lateral photoresistance response decreases with increasing bias step-by-step with clear resistance resolution for different biases. Moreover, although the difference of lateral photoresistances at the positive bias and the negative bias decreases with increasing biases, they are still clearly distinguishable except for that of 10 V, indicating the possibility of the bias modulation for the CIGS heterojunction memory devices. Besides, from the results in Fig. 3d, it is observed that the lateral photoresistance response should also be strongly dependent on the laser wavelength, and then the transient lateral photoresistance response is measured under the 5 mW illumination of different lasers, as shown in Fig. 4d. The clear high and low levels can also be found with well-defined response amplitude. Furthermore, Fig. 5a gives the transient lateral photoresistance curve with laser beam staying at different positions. The lateral photoresistance keeps the constant and stable position dependence, implying that the LPRE can be used to develop the position-dependent resistance memory devices. For memory device, the memory density is thought to be one of the key parameters. In order to judge this factor, we measured the position resolution of the lateral

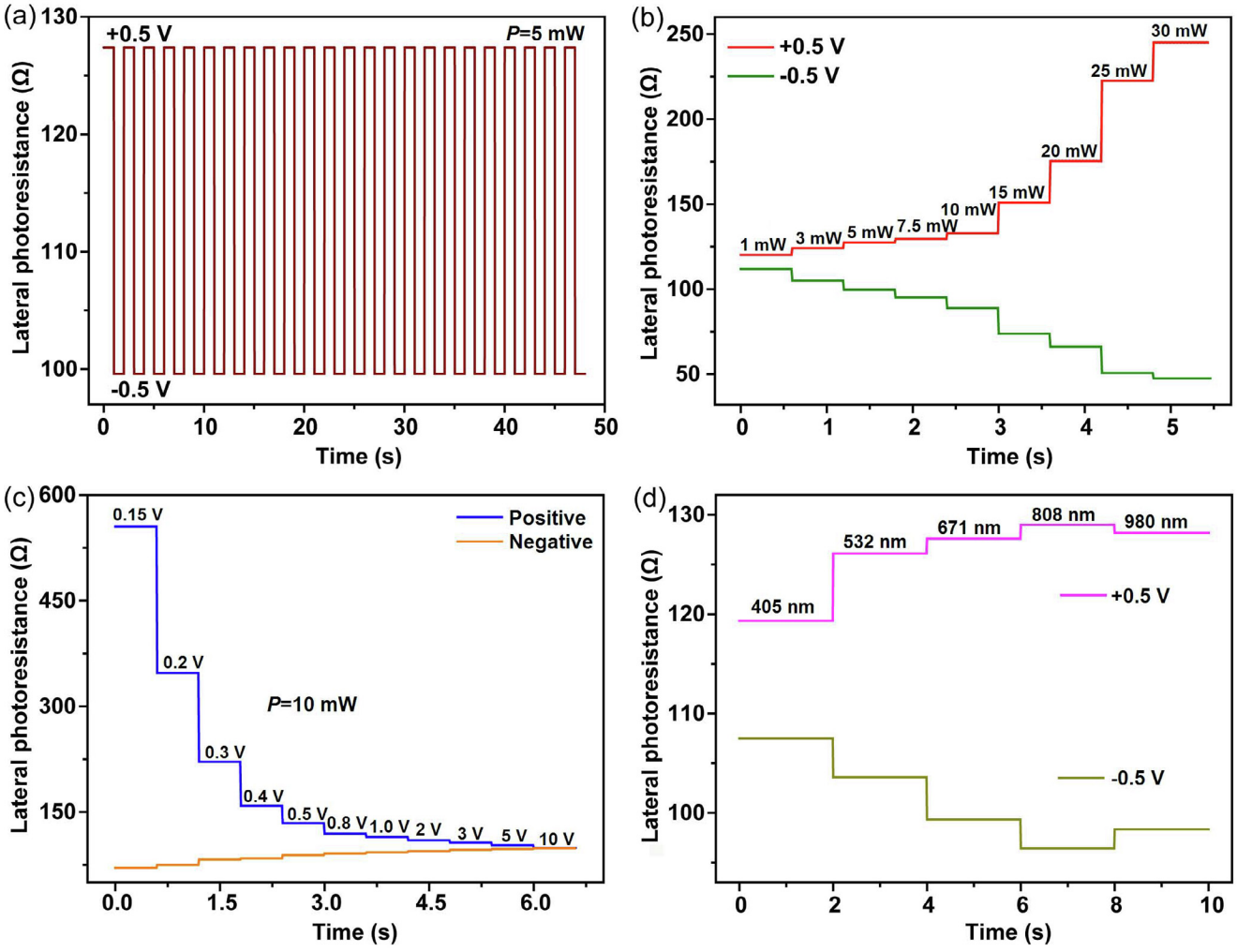


**Fig. 4.** (Color online) The modulation and stability measurements of the lateral photoresistance. (a) The typical time-dependent lateral photoresistance curve with periodic bias of +0.5 and −0.5 V under illumination of 5 mW. The time-dependent lateral photoresistance curves (b) under illumination of different laser powers of a 671 nm-laser, (c) with adding different biases, and (d) under 5 mW illumination of different lasers.

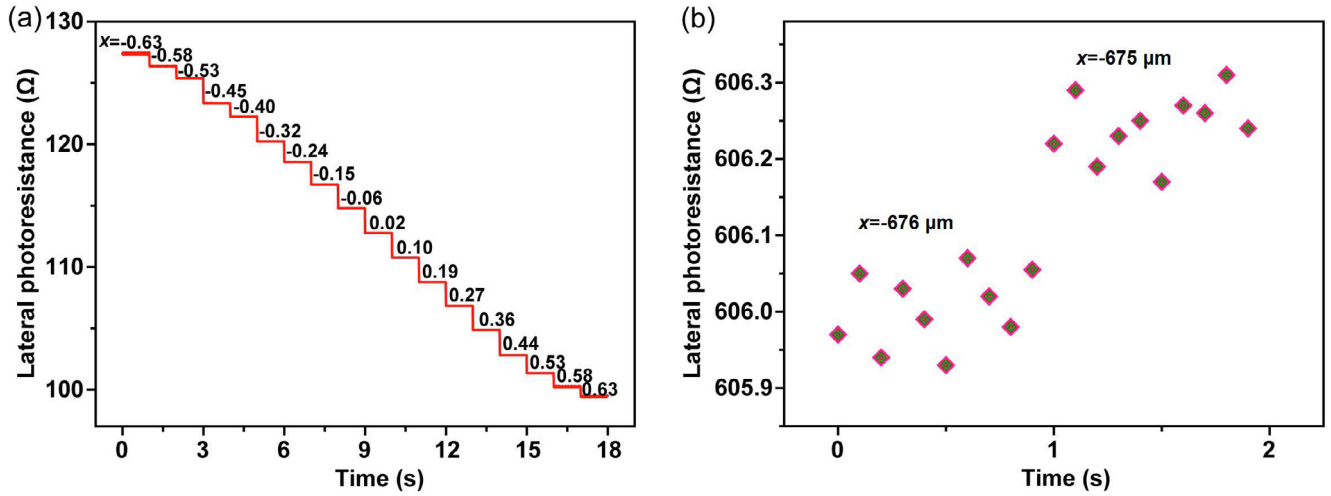


**Fig. 5.** (Color online) The position sensitivity measurements of the lateral photoresistances. (a) The time-dependent lateral photoresistance curve with laser staying at different positions under illumination of 5 mW of a 671 nm-laser. (b) The time-dependent lateral photoresistance response with laser staying at −676 and −675 μm under illumination of 10 mW (bias of 0.15 V).

photoresistances with laser beam moving from −676 to −675 μm (this is the minimum step size of the system), as shown in Fig. 5b. The lateral photoresistance (averaged) at the position of −676 μm is clearly different from that at −675 μm. However, considering the ultralarge laser spot (diameter of ~100 μm), this position resolution may not reflect the best results of the CIGS heterojunction. Notably, one important shortcoming is that this position-dependent photoresistance memory device cannot work without continuous laser illumination due to its typical structure characteristic of this heterostructure, but it still gives an important insight of developing LPRE-based memory device by choosing nonvolatile materials or structures.

In order to explain the working principle of the LPRE in the CIGS multilayer heterojunction, a physical model was built, as shown in Fig. 6a. Under illumination of suitable lasers from the ITO surface, the energy is mainly absorbed by the CIGS, and excites electron-hole pairs there. The carriers are separated and swept to the ITO layer and the Mo layer (as illuminated from the energy band diagram in Fig. 6a), respectively, leading to excess carriers gathering around the laser position, then, the carriers will diffuse. Under one dimensional simplification, the carrier distribution equation $N_\lambda(x)$ can be expressed as

$$N_\lambda(x) = \begin{cases} N_\lambda(0)\exp\left(-\frac{x-x_0}{l_0}\right)(x_0 < x \le L) \\ N_\lambda(0)\exp\left(-\frac{x_0-x}{l_0}\right)(-L \le x < x_0) \end{cases}, \quad (2)$$

where $N_\lambda(x)$ is the distribution density of the carriers at the $x$ position with a $\lambda$ wavelength laser illumination, $x_0$ represents the position of the laser beam, $-L$ and $L$ correspond to the A position and the B position, respectively, $N_\lambda(0)$ is the steady electron density gathered at the laser position, and $l_0$ represents the diffusion length of the carriers. From Fig. 6a, it is observed that the ITO layer can be distinguished as two regions based on the diffusion orientation of the generated carriers (the diffusion orientation is from right to left in the left region of the laser beam, and is from left to right in the right region of the laser beam). Under positive bias, the drifted carriers have the same orientation as that of the diffused carriers in the left region, leading to an enhanced current (small scattering effect) and thus reduced resistance (defined as increasing conductivity region). While in the right region, the diffusion orientation of the carriers is contrary to that of the drift carriers, and the resistance should increase due to the large probability of the carrier' scattering (defined as decreasing conductivity region). It is assumed that the density of the drifted carriers is $n_0$ under no illumination, and the carrier density can be calculated by simply subtracting or adding the density of the diffusion and drift carriers, then the balanced electron density in light can be written as $N(x) = n_0 + N_\lambda(x)$ in the left region, and expressed as $N(x) = n_0 - N_\lambda(x)$ in the right region. Based on the theoretical relationship, the resistivity ($\rho(x)$) is obtained as follows:

$$\rho(x) = \begin{cases} \frac{1}{\left(n_0 + N_\lambda(0)\exp\left(-\frac{x-x_0}{l_0}\right)\right)q\mu_e}(x_0 \le x \le L) \\ \frac{1}{\left(n_0 - N_\lambda(0)\exp\left(-\frac{x_0-x}{l_0}\right)\right)q\mu_e}(-L \le x < x_0) \end{cases}, \quad (3)$$

where $q$ represents the charge quantity, and $\mu_e$ represents the mobility of the electron. From Eq. (3), the resistance ($R(x_0)$) can be written as

$$R(x_0) = \int_{-L}^{L} \rho(x)\mathrm{d}x/S, \quad (4)$$

where $S$ is a coefficient. Combining Eqs. (3) and (4), $L$ is thought to be much smaller than $l_0$, and $N_\lambda(0)$ is supposed to be much smaller than $n_0$, then the resistance can be derived as

$$R(x_0) \approx \left(D + \frac{2N_\lambda(0)}{n_0(V)^2 q\mu_e l_0}\exp\left(\frac{-L}{l_0}\right)x_0\right)/S, \quad (5)$$

where $D = \frac{2L}{n_0 q\mu_e} - \frac{l_0}{n_0 q\mu_e}\ln\left(1 - \frac{N_\lambda^2(0)}{n_0^2}\right)$. Based on Eq. (5), the photoresistance should exhibit a linear dependence on the $x_0$.

Generally, $n_0$ increases linearly with the bias, when the bias gets enough large, $n_0$ increases greatly, so that the scattering effect to it by $N_\lambda(0)$ can be neglected, as illustrated in Fig. 6b, then the Eq. (5) can be rewritten as

$$R(x_0) = \left(\frac{2L}{n_0 q\mu_e}\right)/S. \quad (6)$$

The resistance is an intrinsic parameter of the ITO layer and not related to the illumination power, which may be why the resistance keeps constant under quite large biases. However, when the bias is very small and the laser power is enough large, $N_\lambda(0)$ should be comparable to or even larger than $n_0$, as shown in Fig. 6c. The diffusion current may be enough large to offset the drift current in the right region, leading to the nonlinear behavior with the largely increased photoresistance in the right region and relatively small decreased photoresistance in the left region.

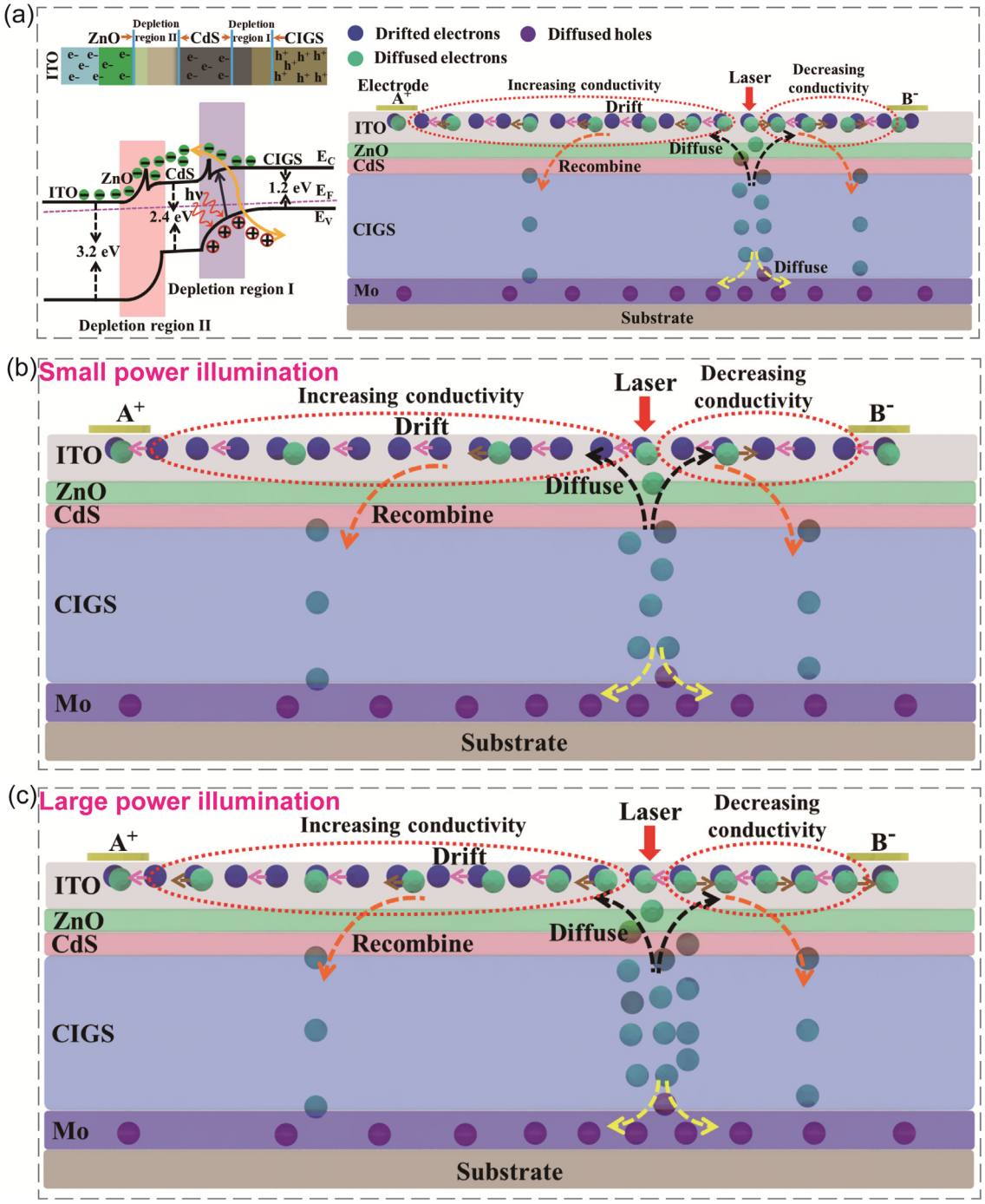


**Fig. 6.** (Color online) The working principle illustration of the LPRE. (a) Band diagram of the CIGS multilayer heterojunction and the corresponding schematic diffusion and drift model of LPRE in the heterojunction. The schematic diffusion and drift model of LPRE under illumination of (b) small powers (or large biases) and (c) large powers (or small biases).

For the dependence of the resistance response on the wavelength, it should be resorted to the quantum efficiency ($\xi$) as $N_\lambda(0)$ is dependent on both $\lambda$ and $\xi$ with the expression of $N_\lambda(0) = \frac{\xi P}{hc}\lambda$, where $P$ represents a laser power, $c$ is the light velocity. With wavelength increasing gradually from 405 to 808 nm, $\xi$ also improves, then the $N_\lambda(0)$ gets largely increased, resulting in the enhanced lateral photoresistance response. While when the wavelength increases again to 980 nm, $\xi$ decreases greatly, thus dominated by $\xi$, $N_\lambda(0)$, as well as the lateral photoresistance response, starts to decrease.

Finally, the time response, as another key factor of an optical sensor [7,30], is studied in the CIGS multilayer heterostructure. The transient resistance response under illumination of a 671 nm-laser with different powers (1 to 30 mW) and applying alternative bias of ±0.5 V at 10 Hz is measured and illustrated in Fig. 7a. The rise(/fall) time, which is evaluated by a time interval of photoresistance rising(/decaying) from 10%(/90%) to 90%(/10%) of the response amplitude, is summarized in Fig. 7b. With illumination power changing from 1 to 30 mW, the rise time ($\tau_{rise}$) decreases slightly from ~15.85 to ~14.40 ms and the fall time ($\tau_{fall}$) reduces from ~15.72 to ~14.37 ms. It seems that the laser power has more or less effect on the response speed of the LPRE, which may be ascribed to the faster scattering rate at larger powers because of the larger number of the separated carriers. Then, the

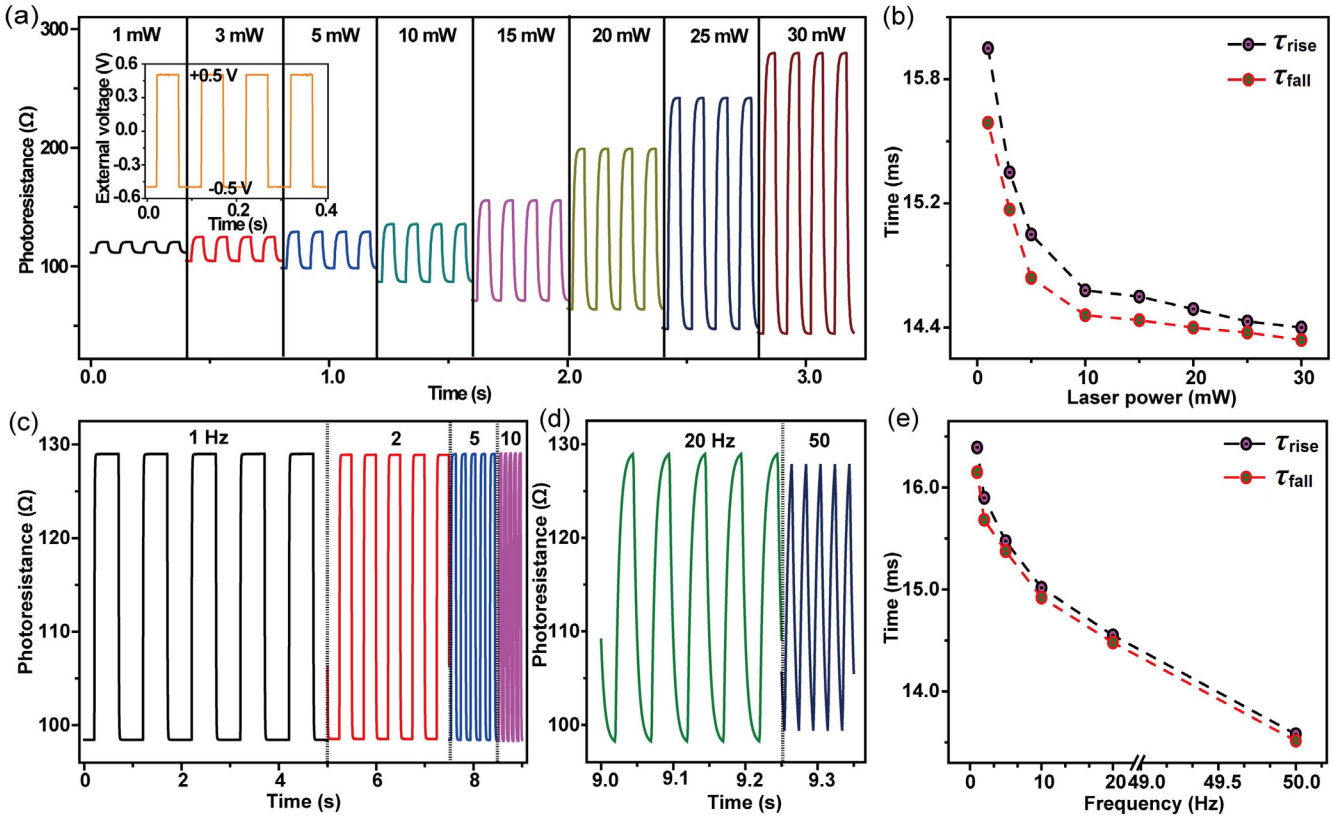


**Fig. 7.** (Color online) The time response measurements of the lateral photoresistance. (a) Time-dependent photoresistance under illumination of different powers (671 nm-laser) with laser position keeping near electrode A, and the inset is the added periodic bias of ±0.5 V at frequency of 10 Hz. (b) The corresponding $\tau_{rise}$ and $\tau_{fall}$ of the PSD as a function of laser power. Time-dependent photoresistance under illumination of a 671-nm laser with 10 mW at frequencies of (c) 1, 2, 5, 10 Hz and (d) 20, 50 Hz. (e) The corresponding $\tau_{rise}$ and $\tau_{fall}$ of the PSD as a function of bias frequency.

time-dependent photoresistance of the CIGS multilayer heterojunction is also well investigated under illumination of 10 mW with frequency increasing from 1 to 50 Hz and the measured results are given in Fig. 7c and d. It is clear that the photoresistance amplitude holds constant at 1 to 20 Hz, but starts to decrease a little with further improving frequency, indicating that the limits of the response speed is located at ~20 Hz. The $\tau_{rise}$ and $\tau_{fall}$ are extracted and plotted in Fig. 7e. The $\tau_{rise}$(/$\tau_{fall}$) decreases from ~16.39(/~16.15 ms) to ~14.46(/~14.42 ms) with the frequency changing from 1 to 20 Hz, and then reduces to 13.58(/13.52 ms) at 50 Hz. As the bias turning on +0.5 or −0.5 V is controlled by an electrical component, the response time of the photoresistance may be influenced by that of the electrical component. However, we do not find any lag of bias response in the frequency range. Therefore, this phenomenon should be attributed to the time resolution differences of different frequencies as the resolution is a little higher at larger measurement frequency and the extracted response speed is more accuracy [7,36]. However, considering the reduced lateral photoresistance response at larger frequencies, the actual response times should be ~14.46 and ~14.42 ms at 20 Hz.

## 4. Conclusion

In conclusion, we first studied the LPRE in the CIGS-based multilayer heterojunction and successfully developed it as a photoresistance-based PSD and position-dependent photoresistance memory device. This heterojunction PSD exhibits very excellent dipolar LPRE performances with position sensitivity of ~63.26 Ω/mm, nonlinearity no more than 4.5%, broadband spectra range (~330 to ~1150 nm), and fast response speed (~14.46/~14.42 ms). Moreover, it is also observed that the LPRE response and nonlinearity of the PSD can be effectively modulated based on the applied bias voltages and illumination powers. While, for the position-dependent resistance memory device, it can be worked by changing laser intensity, wavelength, and bias voltage with excellent stability, repeatability, and excellent memory density. These results can be well explained according to the diffusion and drift model of carriers in the CIGS multilayer heterojunction. Our study uncovers the great potential of LPRE in the CIGS multilayer heterojunction as photoelectric sensors, and also provides a new ideal of developing other materials or structures as photoresistance-modulated PSDs and memory devices.

## Conflict of interest

The authors declare that they have no conflict of interest.

## Acknowledgments

This work was supported by the National Natural Science Foundation of China (11704094, 11504076, 51372064, 61405040, 51622205, 61675027, 51432005, and 61505010), the Natural Science Foundation of Hebei Province (F2019201047, F2018201198, F2017201141, and E2017201227), the Natural Science Foundation for Distinguished Young Scholars of Hebei University (2015JQ03), and Young Talents of Hebei Province.

## Author contributions

Shuang Qiao, Shufang Wang, and Caofeng Pan designed and supervised the work. Jihong Liu and Zicai Zhang carried out the LPRE measurements and prepared the data. All authors performed

the data analysis and discussions. Shuang Qiao, Jihong Liu and Zicai Zhang wrote the manuscript. All authors read and commented on the manuscript.

## Appendix A. Supplementary materials

Supplementary materials to this article can be found online at https://doi.org/10.1016/j.scib.2019.11.016.

## References


[1] Han X, Du WM, Yu RM, et al. Piezo-phototronic enhanced UV sensing based on a nanowire photodetector array. Adv Mater 2015;27:7963–9.
[2] Pan CF, Chen MX, Yu RM, et al. Progress in piezo-phototronic effect enhanced light-emitting diode and pressure imaging. Adv Mater 2016;28:1535–52.
[3] Wang XD, Que ML, Chen MX, et al. Full dynamic-range pressure sensor matrix based on optical and electrical dual-mode sensing. Adv Mater 2017;29:1605817.
[4] Wang XD, Zhang YF, Zhang XJ, et al. A highly stretchable transparent self-powered triboelectric tactile sensor with metallized nanofibers for wearable electronics. Adv Mater 2018;30:1706738.
[5] Hu GF, Zhou RR, Yu RM, et al. Piezotronic effect enhanced Schottky-contact ZnO micro/nanowire humidity sensor. Nano Res 2014;7:1083–91.
[6] Li XY, Chen MX, Yu RM, et al. Enhancing light emission of ZnO-nanofilm/Si-micropillar heterostructure arrays by piezo-phototronic effect. Adv Mater 2015;27:4447–53.
[7] Cong RD, Qiao S, Liu J, et al. Ultrahigh, ultrafast, and self-powered visible-near-infrared optical position-sensitive detector based on a CVD-prepared vertically standing few-layer $MoS_2$/Si heterojunction. Adv Sci 2018;5:1700502.
[8] Mashkoor A, Din R, Pan C, et al. Investigation of dydrogen storage capabilities of ZnO-based nanostructures. J Phys Chem C 2010;114:2560–5.
[9] Wang ZR, Wang H, Liu B, et al. Transferable and flexible nanorod-assembled $TiO_2$ cloths for dye-sensitized solar cells, photodetectors, and photocatalysts. ACS Nano 2011;5:8412.
[10] Dou LT, Yang Y, You JB, et al. Solution-processed hybrid perovskite photodetectors with high detectivity. Nat Commun 2014;5:5404.
[11] Qiao S, Liu YN, Liu JH, et al. The reverse lateral photovoltaic effect in boron-diffused Si pn junction structure. IEEE Electron Device Lett 2016;37:201.
[12] Liu JH, Qiao S, Liang BL, et al. Lateral photovoltaic effect observed in doping-modulated GaAs/$Al_{0.3}Ga_{0.7}As$. Opt Express 2017;25:A166–75.
[13] Jaffe JE, Zunger A. Anion displacements and the band-gap anomaly in ternary chalcopyrite semiconductors. Phys Rev B 1983;27:5176.
[14] Qiao S, Liu JH, Niu XN, et al. Piezophototronic effect enhanced photoresponse of the flexible Cu(In, Ga)$Se_2$ (CIGS) heterojunction photodetectors. Adv Funct Mater 2018;28:1707311.
[15] Theodoropoulou S, Papadimitriou D, Anestou K, et al. Optical properties of $CuIn_{1-x}Ga_xSe_2$ quaternary alloys for solar-energy conversion. Semicond Sci Technol 2009;24:015014.
[16] Kaelin M, Rudmann D, Tiwari AN, et al. Low cost processing of CIGS thin film solar cells. Sol Energy 2004;77:749–56.
[17] Jackson P, Wuerz R, Hariskos D, et al. Effects of heavy alkali elements in Cu(In, Ga)$Se_2$ solar cells with efficiencies up to 22.6%. Phys Status Solidi RRL 2016;10:583.
[18] McDonald SA, Konstantatos G, Zhang SG, et al. Solution-processed PbS quantum dot infrared photodetectors and photovoltaics. Nat Mater 2005;4:138–42.
[19] Schottky W. On the origins of photoelectrons in $Cu_2O$-Cu photocells. Phys Z 1930;31:913.
[20] Henry J, Livingstone J. Sputtered a-Si: H thin-film position sensitive detectors. J Phys D: Appl Phys 2001;34:1939.
[21] Yu CQ, Wang H, Xia YX, et al. Enhanced lateral photovoltaic effect in an improved oxide-metal-semiconductor structure of $TiO_2$/Ti/Si. Appl Phys Lett 2009;95:263506.
[22] Zhao K, Jin KJ, Lu HB, et al. Transient lateral photovoltaic effect in p-n heterojunctions of $La_{0.7}Sr_{0.3}MnO_3$ and Si. Appl Phys Lett 2006;88:141914.
[23] Jin KJ, Zhao K, Lu HB, et al. Dember effect induced photovoltage in perovskite p-n heterojunctions. Appl Phys Lett 2007;91:081906.
[24] Wang XJ, Zhao XF, Hu C, et al. Large lateral photovoltaic effect with ultrafast relaxation time in SnSe/Si junction. Appl Phys Lett 2016;109:023502.
[25] Wang WH, Yan ZZ, Zhang JF, et al. High-performance position-sensitive detector based on grapheme-silicon heterojunction. Optica 2018;5:27–31.
[26] Qiao S, Feng KY, Li ZQ, et al. Ultrahigh, ultrafast and large response size visible-near-infrared optical position sensitive detectors based on CIGS structures. J Mater Chem C 2017;5:4915–22.
[27] Yu CQ, Wang H. Light-induced bipolar-resistance effect based on metal-oxide-semiconductor structures of Ti/$SiO_2$/Si. Adv Mater 2010;22:966–70.
[28] Gan ZK, Zhou PQ, Huang X, et al. Dual modulated lateral photoresistance effect observed on silicon-based discontinuous copper film. Adv Electron Mater 2017;3:1700293.
[29] Henry J, Livingstone J. Thin-film amorphous silicon position-sensitive detectors. Adv Mater 2001;13:1023.
[30] Yu CQ, Wang H. Large lateral photovoltaic effect in metal-(oxide-) semiconductor structures. Sensors 2010;10:10155–80.
[31] Fortunato E, Lavareda G, Martins R, et al. Large-area 1D thin-film position-sensitive detector with high detection resolution. Sens Actuators A 1996;51:135–42.
[32] Qiao S, Liu JH, Fu G, et al. ZnO nanowire based CIGS solar cell and its efficiency enhancement by the piezo-phototronic effect. Nano Energy 2018;49:508–14.
[33] Ogawa S, Naijo T, Kimura Y, et al. Photoinduced doping effect of pentacene field effect transistor in oxygen atmosphere studied by displacement current measurement. Appl Phys Lett 2005;86:252104.
[34] Guo WX, Xu C, Zhu G, et al. Optical-fiber/$TiO_2$-nanowire-arrays hrbrid structures with tubular counterelectrode for dye-sensitized solar cell. Nano Energy 2012;1:176–82.
[35] Pan CF, Luo ZX, Xu C, et al. Wafer-scale high-throughput ordered arrays of Si and coaxial Si/$Si_{1-x}Ge_x$ wires: fabrication, characterization, and photovoltaic application. ACS Nano 2011;5:6629–36.
[36] Qiao S, Cong RD, Liu JH, et al. A vertically layered $MoS_2$/Si heterojunction for an ultrahigh and ultrafast photoresponse photodetector. J Mater Chem C 2018;6:3233–329.


Jihong Liu received her Master degree in College of Physics and Information Engineering, Hebei Normal University in 2008, and joined in College of Physics Science and Technology, Hebei University in 2014. Her research focuses on the fields of preparation of solar cells and the optoelectronic/photovoltaic performances of semiconductor heterostructures.

Shuang Qiao received his Ph.D. degree in Institute of Semiconductors, Chinses Academy of Sciences in 2014. He then worked in College of Physics Science and Technology, Hebei University and became an Associated Professor in 2016. Since 2017, he has been a visiting fellow in the group of Prof. Caofeng Pan at Beijing Institute of Nanoenergy and Nanosystems, Chinese Academy of Sciences. His research focuses on the fields of fabrication of novel semiconductor heterostructures, optoelectronic/photovoltaic properties, ultrafast dynamics, and piezo-phototronic effect of nano devices.

Shufang Wang received her Ph.D. degree in Optics from the Institute of Physics, Chinese Academy of Sciences in 2004. She then joined in the group of Prof. D. Rémiens at IEMN-CNRS, France as a postdoctral fellow and after that joined in the group of Prof. Xiaoxing Xi at the Penn. State University as a postdoctral fellow. She is currently a full Professor and a group leader at Hebei University. Her researches focus on the fields of phototelectric/the rmalelectric materials and devices.

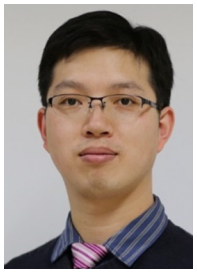

Caofeng Pan received his B.S. (2005) and Ph.D. (2010) degrees in Materials Science and Engineering from Tsinghua University. He then joined the Georgia Institute of Technology as a postdoctoral fellow. He is currently a Professor and a group leader at Beijing Institute of Nanoenergy and Nanosystems, Chinese Academy of Sciences. His main research interests focus on the fields of piezotronics/piezo-phototronics for fabricating new electronic and optoelectronic devices, nano-power source (such as nanofuel cell, nano biofuel cell and nanogenerator), hybrid nanogenerators, and self-powered nanosystems.